PERGAMON

International Journal of Hydrogen Energy 25 (2000) 669–683

International Journal of HYDROGEN ENERGY

Novel inorganic hydride

Randell L. Mills*

BlackLight Power, Inc., 493 Old Trenton Road, Cranbury, NJ 08512, USA

Abstract

A novel inorganic hydride compound KH $KHCO_3$ which is stable in water and comprises a high binding energy hydride ion was isolated following the electrolysis of a K_2CO_3 electrolyte. Inorganic hydride clusters $K[KH\ KHCO_3]_n^+$ were identified by Time of Flight Secondary Ion Mass Spectroscopy. Moreover, the existence of a novel hydride ion has been determined using X-ray photoelectron spectroscopy, and proton nuclear magnetic resonance spectroscopy. Hydride ions with increased binding energies may be the basis of a high voltage battery for electric vehicles.

1. Introduction

Evidence of the changing landscape for automobiles can be found in the recent increase in research into the next generation of automobiles. But, the fact that there is no clear front-runner in the technological race to replace the internal combustion (IC) engine can be attested to by the divergent approaches taken by the major automobile companies. Programs include various approaches to hybrid vehicles, alternative fueled vehicles such as dual-fired engines that can run on gasoline or compressed natural gas, and a natural gas-fired engine. Serious efforts are also being put into a number of alternative fuels such as ethanol, methanol, propane, and reformulated gasoline. To date, the most favored approach is an electric vehicle based on fuel cell technology or advanced battery technology such as sodium nickel chloride, nickel-metal hydride, and lithium-ion batteries [1]. Although billions of dollars are being spent to develop an alternative to the IC engine, there is no technology in sight that can match the specifications of an IC engine system [2].

Fuel cells have advantages over the IC engine because they convert hydrogen to water at about 70% efficiency when running at about 20% below peak output [3]. But, hydrogen is difficult and dangerous to store. Cryogenic, compressed gas, and metal hydride storage are the main options. In the case of cryogenic storage, liquefaction of hydrogen requires an amount of electricity which is at least 30% of the lower heating value of liquid hydrogen [4]. Compressed hydrogen, and metal hydride storage are less viable since the former requires an unacceptable volume, and the latter is heavy and has difficulties supplying hydrogen to match a load such as a fuel cell [4]. The main challenge with hydrogen as a replacement to gasoline is that a hydrogen production and refueling infrastructure would have to be built. Hydrogen may be obtained by reforming fossil fuels. However, in practice fuel cell vehicles would probably achieve only 10–45% efficiency because the process of reforming fossil fuel into hydrogen and carbon dioxide requires energy [3]. Presently, fuel cells are also impractical due to their high cost as well as the lack of inexpensive reforming technology [5].

* Tel.: +1-609-490-1040; fax: +1-609-490-1066.
E-mail address: rmills@blacklightpower.com (R.L. Mills).

0360-3199/00/$20.00
PII: S0360-3199(99)00076-2

In contrast, batteries are attractive because they can be recharged wherever electricity exists, which is ubiquitous. The cost of mobile energy from a battery powered car may be less than that from a fossil fuel powered car. For example, the cost of energy per mile of a nickel metal hydride battery powered car is 25% of that of a IC powered car [6]. However, current battery technology is trying to compete with something that it has little chance of imitating. Whichever battery technology proves to be superior, no known electric power plant will match the versatility and power of an internal combustion engine. A typical IC engine yields more than 10,000 W h kg^{-1} of energy, while the most promising battery technology yields 200 W h kg^{-1} [2].

A high voltage battery would have the advantages of much greater power and much higher energy density. The limitations of battery chemistry may be attributed to the binding energy of the anion of the oxidant. For example, the 2 V provided by a lead acid cell is limited by the 1.46 eV electron affinity of the oxide anion of the oxidant PbO_2. An increase in the oxidation state of lead such as $Pb^{2+} \rightarrow Pb^{3+} \rightarrow Pb^{4+}$ is possible in a plasma. Further oxidation of lead could also be achieved in theory by electrochemical charging. However, higher lead oxidation states are not achievable because the oxide anion required to form a neutral compound would undergo oxidation by the highly oxidized lead cation. An anion with an extraordinary binding energy is required for a high voltage battery. One of the highest voltage batteries known is the lithium fluoride battery with a voltage of about 6 V. The voltage can be attributed to the higher binding energy of the fluoride ion. The electron affinity of halogens increases from the bottom of the Group VII elements to the top. A hydride ion may be considered a halide since it possesses the same electronic structure, and, according to the binding energy trend, it should have a high binding energy. However, the binding energy is only 0.75 eV which is much lower than the 3.4 eV binding energy of a fluoride ion.

An inorganic hydride compound having the formula KH $KHCO_3$ was isolated from an aqueous K_2CO_3 electrolytic cell reactor. Inorganic hydride clusters $K[KH\,KHCO_3]_n^+$ were identified by Time of Flight Secondary Ion Mass Spectroscopy (ToF-SIMS). A hydride ion with a binding energy of 22.8 eV has been observed by X-ray photoelectron spectroscopy (XPS) having upfield shifted solid state magic-angle spinning proton nuclear magnetic resonance (^{1}H MAS NMR) peaks. Moreover, a polymeric structure is indicated by Fourier transform infrared (FTIR) spectroscopy. The discovery of a novel hydride ion with a high binding energy has implications for a new field of hydride chemistry with applications such as a high voltage battery. Such extremely stable hydride ions may stabilize positively charged ions in an unprecedented highly charged state. A battery may be possible having projected specifications that surpass those of the internal combustion engine.

Hydride ions having extraordinary binding energies may stabilize a cation M^{x+} in an extraordinarily high oxidation state such as +2 in the case of lithium. Thus, these hydride ions may be used as the basis of a high voltage battery of a rocking chair design wherein the hydride ion moves back and forth between the cathode and anode half cells during discharge and charge cycles. Exemplary reactions for a cation M^{x+} are:

Cathode reaction

$$MH_x + e^- \rightarrow MH_{x-1} + H^- \quad (1)$$

Anode reaction

$$MH_{x-2} + H^- \rightarrow MH_{x-1} + e^- \quad (2)$$

Overall reaction

$$MH_x + MH_{x-2} \rightarrow 2MH_{x-1} \quad (3)$$

2. Experimental

2.1. Synthesis

An electrolytic cell comprising a K_2CO_3 electrolyte, a nickel wire cathode, and platinized titanium anodes was used to synthesize the KH $KHCO_3$ sample [7]. Briefly, the cell vessel comprised a 10 gallon (33″ × 15″) Nalgene tank. An outer cathode comprised 5000 m of 0.5 mm diameter clean, cold drawn nickel wire (Ni 200 0.0197″, HTN36NOAG1, A-1 Wire Tech, Inc., Rockford, Illinois, 61109) wound on a polyethylene cylindrical support. A central cathode comprised 5000 m of the nickel wire wound in a toroidal shape. The central cathode was inserted into a cylindrical, perforated polyethylene container that was placed inside the outer cathode with an anode array between the central and outer cathodes. The anode comprised an array of 15 platinized titanium anodes (ten Engelhard Pt/Ti mesh 1.6″ × 8″ with one 3/4″ × 7″ stem attached to the 1.6″ side plated with 100 U series 3000; and five Engelhard 1″ diameter × 8″ length titanium tubes with one 3/4″ × 7″ stem affixed to the interior of one end and plated with 100 U Pt series 3000). Before assembly, the anode array was cleaned in 3 M HCl for 5 min and rinsed with distilled water. The cathode was cleaned by placing it in a tank of 0.57 M K_2CO_3/3% H_2O_2 for 6 h and then rinsing it with distilled water. The anode was placed in the support between the central and outer cathodes, and the electrode assembly was placed in the tank containing electrolyte. The elec-

trolyte solution comprised 28 l of 0.57 M K_2CO_3 (Alfa K_2CO_3 99%). Electrolysis was performed at 20 A constant current with a constant current (±0.02%) power supply.

Samples were isolated from the electrolytic cell by concentrating the K_2CO_3 electrolyte about six-fold using a rotary evaporator at 50°C until a yellow-white polymeric suspension formed. Precipitated crystals of the suspension were then grown over 3 weeks by allowing the saturated solution to stand in a sealed round bottom flask at 25°C. Control samples utilized in the following experiments contained K_2CO_3 (99%), $KHCO_3$ (99.99%), HNO_3 (99.99%), and KH (99%).

2.2. ToF-SIMS characterization

The crystalline samples were sprinkled onto the surface of double-sided adhesive tapes and characterized using a Physical Electronics TFS-2000 ToF-SIMS instrument. The primary ion gun utilized a $^{69}Ga^+$ liquid metal source. In order to remove surface contaminants and expose a fresh surface, the samples were sputter cleaned for 30 s using a 40 μm × 40 μm raster.

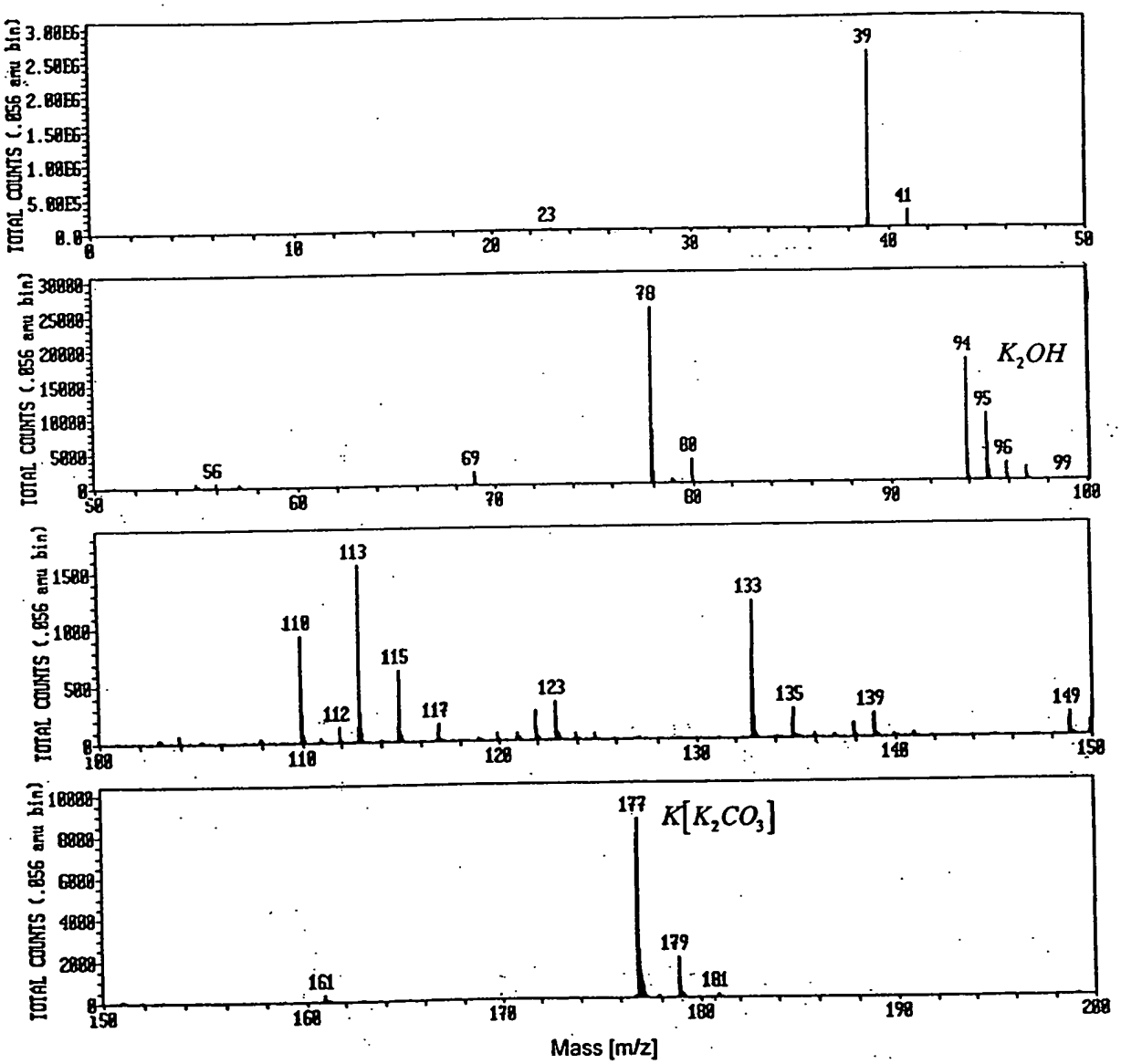

Fig. 1. The positive ToF-SIMS spectrum (*m/e* = 0–200) of $KHCO_3$ (99.99%) where HC is hydrocarbon.

The aperture setting was 3, and the ion current was 600 pA resulting in a total ion dose of 10^{15} ions/cm^2.

During acquisition, the ion gun was operated using a bunched (pulse width 4 ns bunched to 1 ns) 15 kV beam [8,9]. The total ion dose was 10^{12} ions/cm^2. Charge neutralization was active, and the post accelerating voltage was 8000 V. Three different regions on each sample of (12 μm)^2, (18 μm)^2, and (25 μm)^2 were analyzed. The positive and negative SIMS spectra were acquired. Representative post sputtering data is reported.

2.3. XPS characterization

A series of XPS analyses were made on the crystalline samples using a Scienta 300 XPS Spectrometer. The fixed analyzer transmission mode and the sweep acquisition mode were used. The step energy in the survey scan was 0.5 eV, and the step energy in the high resolution scan was 0.15 eV. In the survey scan, the time per step was 0.4 s, and the number of sweeps was 4. In the high resolution scan, the time per step was 0.3 s, and the number of sweeps

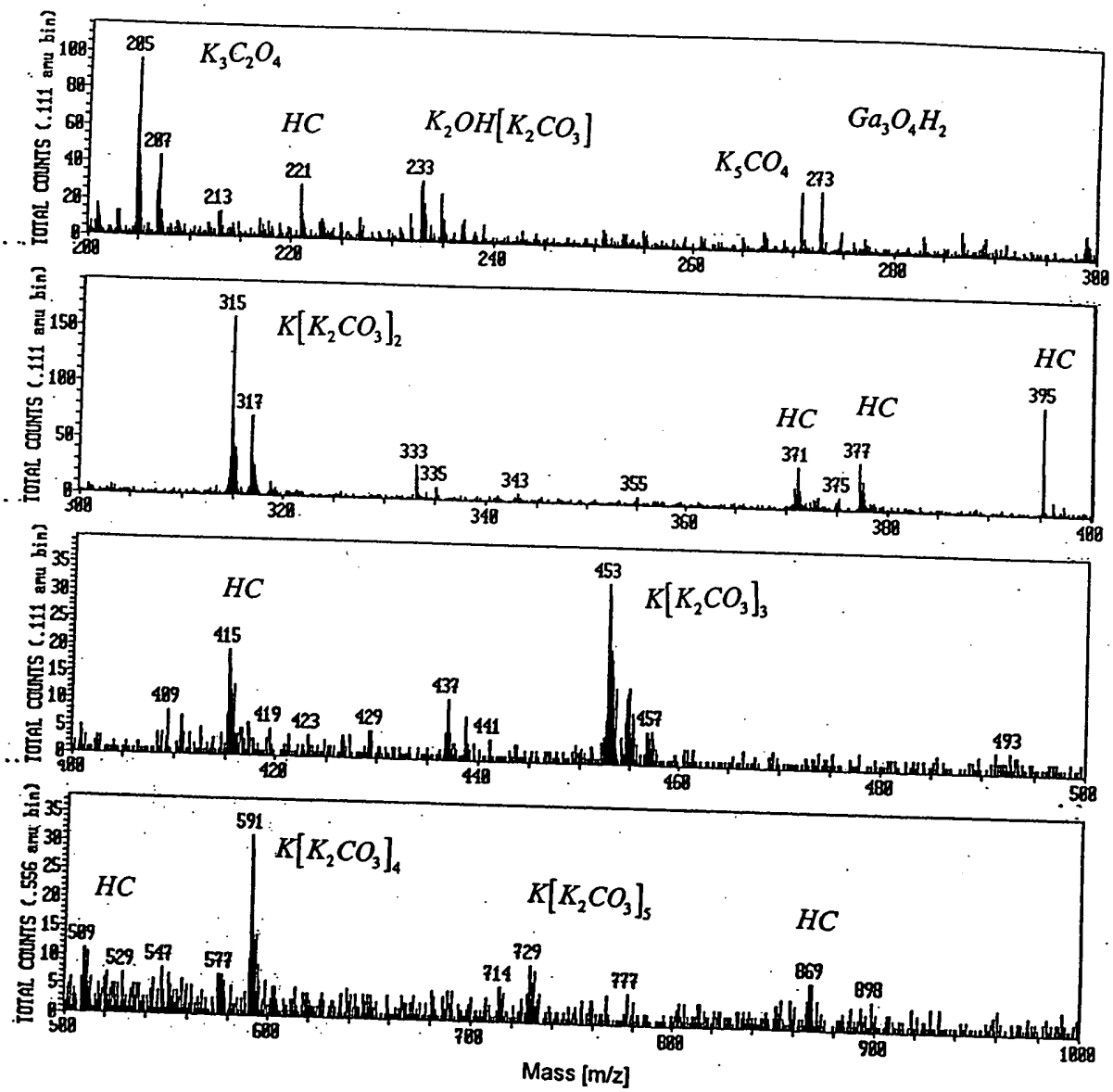

Fig. 2. The positive ToF-SIMS spectrum (m/e = 200–1000) of $KHCO_3$ (99.99%) where HC is hydrocarbon.

was 30. C 1s at 284.6 eV was used as the internal standard.

2.4. NMR spectroscopy

^{1}H MAS NMR was performed on the crystalline samples. The data were obtained on a custom built spectrometer operating with a Nicolet 1280 computer. Final pulse generation was from a tuned Henry radio amplifier. The ^{1}H NMR frequency was 270.6196 MHz. A 2 μs pulse corresponding to a 15° pulse length and a 3-s recycle delay were used. The window was ±31 kHz. The spin speed was 4.5 kHz. The number of scans was

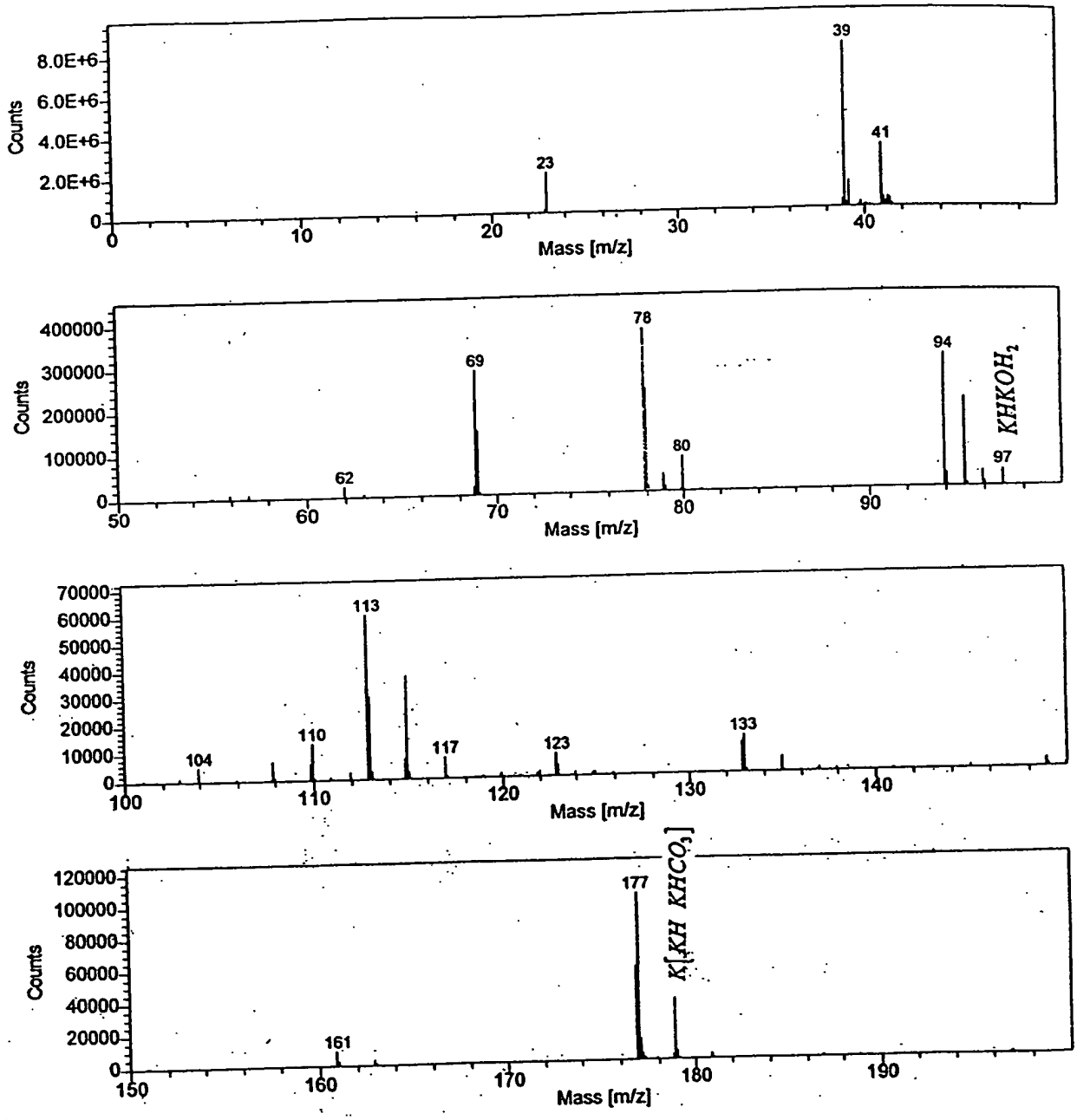

Fig. 3. The positive ToF-SIMS spectrum (m/e = 0–200) of an electrolytic cell sample where HC is hydrocarbon.

Table 1
The respective hydride compounds and mass assignments (m/z) of the positive ToF-SIMS of an electrolytic cell sample

Hydrino hydride compound or fragment	Nominal mass m/z	Observed m/z	Calculated m/z	Difference between observed and calculated m/z
KH	40	39.97	39.971535	0.0015
K_2H	79	78.940	78.935245	0.004
$(KH)_2$	80	79.942	79.94307	0.001
$KHKOH_2$	97	96.945	96.945805	0.0008
$KH_2(KH)_2$	121	120.925	120.92243	0.003
KH $KHCO_2$	124	123.925	123.93289	0.008
KH_2KHO_4	145	144.92	144.930535	0.010
$K(KOH)_2$	151	150.90	150.8966	0.003
$KH(KOH)_2$	152	151.90	151.904425	0.004
$KH_2(KOH)_2$	153	152.90	152.91225	0.012
K[KH $KHCO_3$]	179	178.89	178.8915	0.001
$KCO(KH)_3$	187	186.87	186.873225	0.003
$K_2OHKHKOH$	191	190.87	190.868135	0.002
$KH_2KOHKHKOH$	193	192.89	192.883785	0.006
$K_3O(H_2O)_4$	205	204.92	204.92828	0.008
$K_2OH[KH\ KHCO_3]$	235	234.86	234.857955	0.002
$K[H_2CO_4\ KH\ KHCO_3]$	257	256.89	256.8868	0.003
$K_3O[KH\ KHCO_3]$	273	272.81	272.81384	0.004
$[KH_2CO_3]_3$	303	302.88	302.89227	0.012
$K[KH\ KHCO_3K_2CO_3]$	317	316.80	316.80366	0.004
$K[KH\ KHCO_3]_2$	319	318.82	318.81931	0.001
$KH_2[KH\ KOH]_3$	329	328.80	328.7933	0.007
$KOH_2[KH\ KHCO_3]_2$	337	336.81	336.82987	0.020
$KH\ KO_2\ [KH\ KHCO_3][KHCO_3]$	351	350.81	350.80913	0.001
$KKHK_2CO_3\ [KH\ KHCO_3]$	357	356.77	356.775195	0.005
$KKH[KH\ KHCO_3]_2$	359	358.78	358.790845	0.011
$K_2OH[KH\ KHCO_3]_2$	375	374.78	374.785755	0.005
$K_2OH[KHKOH]_2\ [KHCO_3]$	387	386.75	386.76238	0.012
$KKH_3KH_5[KH\ KHCO_3]_2$	405	404.79	404.80933	0.019
$K_3O[K_2CO_3]\ [KH\ KHCO_3]$ or $K[KH\ KOH(K_2CO_3)_2]$	411	410.75	410.72599	0.024
$K_3O[KH\ KHCO_3]_2$	413	412.74	412.74164	0.002
$K\begin{bmatrix} KH\ KOH \\ (KH\ KHCO_3)_2 \end{bmatrix}$	415	414.74	414.75729	0.017
$KH_2OKHCO_3\ [KH\ KHCO_3]_2$	437	436.81	436.786135	0.024
$KKHKCO_2[KH\ KHCO_3]_2$	442	441.74	441.744375	0.004
$K[KH\ KHCO_3]_3$	459	458.72	458.74711	0.027
$H[KH\ KOH]_2[K_2CO_3]_2$ or $K_4O_2H[KH\ KHCO_3]_2$	469	468.70	468.708085	0.008
$K[K_2CO_3][KHCO_3]_3$	477	476.72	476.744655	0.025
$K_2OH[KH\ KHCO_3]_3$	515	514.72	514.713555	0.006
$K_3O[KH\ KHCO_3]_3$	553	552.67	552.66944	0.001
$K[KH\ KHCO_3]_4$	599	598.65	598.67491	0.025
$K_2OH[KH\ KHCO_3]_4$	655	654.65	654.641355	0.009
$K_3O[KH\ KHCO_3]_4$	693	692.60	692.59724	0.003
$K[KH\ KHCO_3]_5$	739	738.65	738.60271	0.047
$K_3O[KH\ KHCO_3]_5$	833	832.50	832.52504	0.025
$K[KH\ KHCO_3]_6$	879	878.50	878.53051	0.031
$K_3O[KH\ KHCO_3]_6$	973	972.50	972.45284	0.047

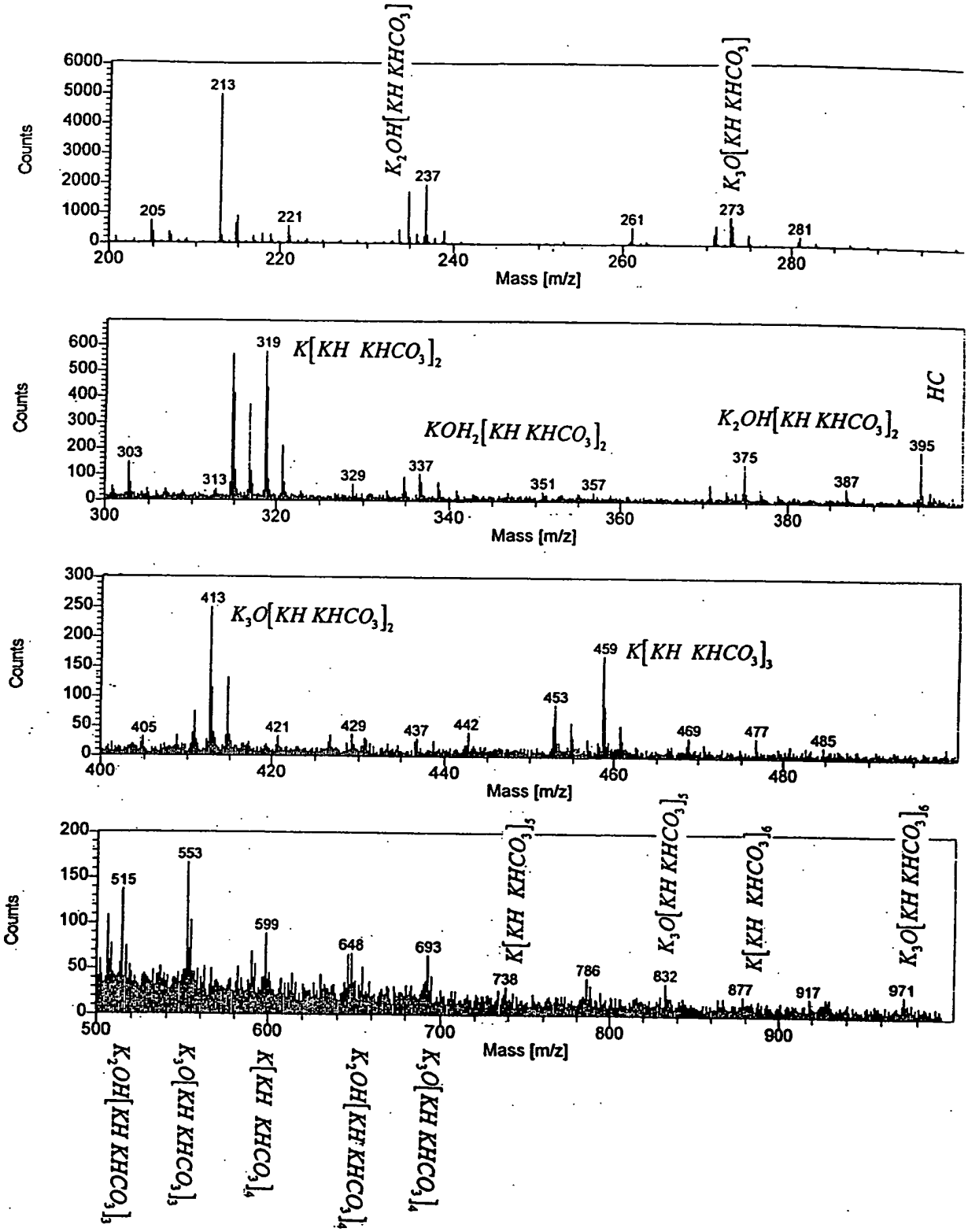

Fig. 4. The positive ToF-SIMS spectrum (m/e = 200–1000) of an electrolytic cell sample where HC is hydrocarbon.

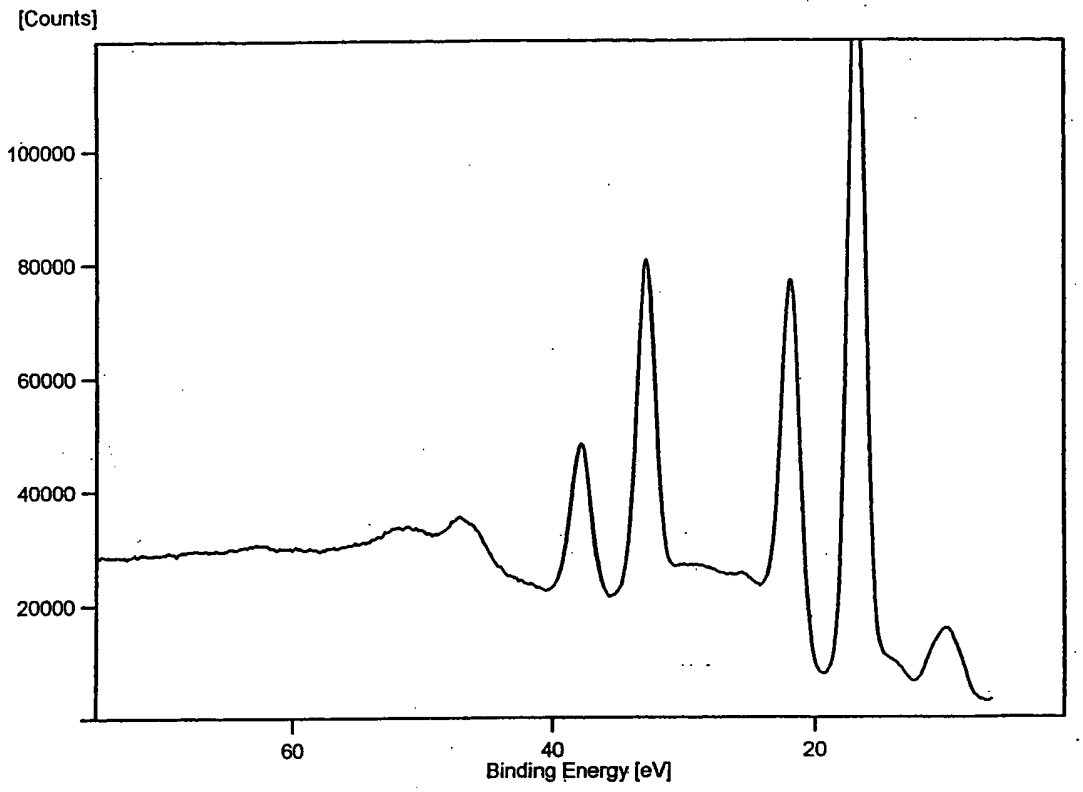

Fig. 5. The 0–80 eV binding energy region of a high resolution XPS spectrum of an electrolytic cell sample.

1000. Chemical shifts were referenced to external TMS. The offset was 1527.12 Hz, and the magnetic flux was 6.357 T.

2.5. FTIR spectroscopy

Samples were transferred to an infrared transmitting substrate and analyzed by FTIR spectroscopy using a Nicolet Magna 550 FTIR Spectrometer with a NicPlan FTIR microscope. The number of scans was 500 for both the sample and background. The number of background scans was 500. The resolution was 8.000. A dry air purge was applied.

3. Results and discussion

3.1. ToF-SIMS

The positive ToF-SIMS spectrum obtained from the $KHCO_3$ control is shown in Figs. 1 and 2. In addition, the positive ToF-SIMS of a sample isolated from the electrolytic cell is shown in Figs. 3 and 4. The respective hydride compounds and mass assignments appear in Table 1. In both the control and electrolytic samples, the positive ion spectrum are dominated by the K^+ ion. Two series of positive ions $K[K_2CO_3]_n^+$ $m/z=(39+138n)$, $K_2OH[K_2CO_3]_n^+$ $m/z=(95+138n)$} are observed in the $KHCO_3$ control. Other peaks containing potassium include KC^+, $K_xO_y^+$, $K_xO_yH_z^+$, KCO^+, and K_2^+. However, in the electrolytic cell sample, three new series of positive ions are observed at $K[KH\,KHCO_3]_n^+$ $m/z=(39+140n)$, $K_2OH[KH\,KHCO_3]_n^+$ $m/z=(95+140n)$, and $K_3O[KH\,KHCO_3]_n^+$, $m/z=(133+140n)$}. These ions correspond to inorganic clusters containing novel hydride combinations (i.e. KH $KHCO_3$ units plus other positive fragments).

The comparison of the positive ToF-SIMS spectrum of the $KHCO_3$ control with the electrolytic cell sample shown in Figs. 1 and 2, and 3 and 4, respectively, demonstrates that the $^{39}K^+$ peak of the electrolytic cell sample may saturate the detector and give rise to a peak that is atypical of the natural abundance of ^{41}K. The natural abundance of ^{41}K is 6.7%; whereas, the observed ^{41}K abundance from the electrolytic cell sample is 57%. This atypical abundance was also confirmed using ESIToFMS [10]. The high resolution mass assignment of the m/z = 41 peak of the electrolytic sample was consistent with ^{41}K, and no peak was observed at m/z = 42.98 ruling out $^{41}KH_2^+$. Moreover,

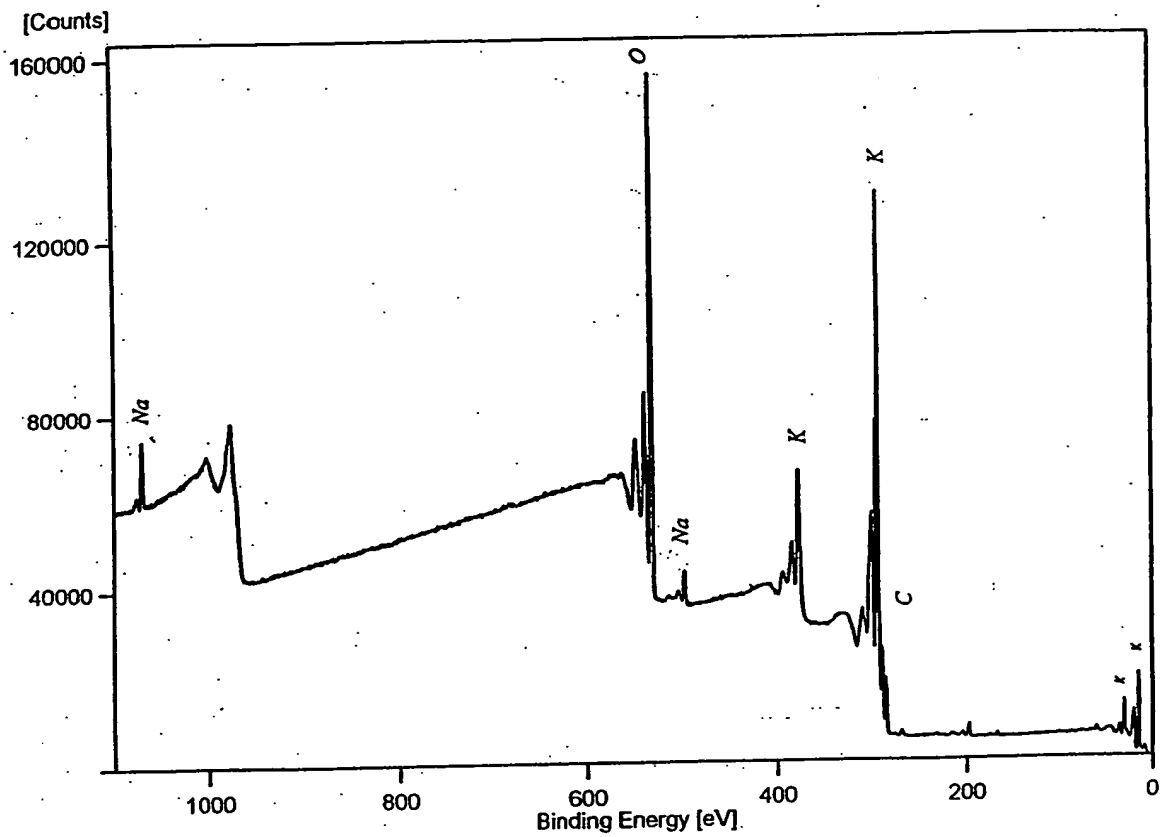

Fig. 6. The XPS survey spectrum of an electrolytic cell sample with the primary elements identified.

the natural abundance of ^{41}K was observed in the positive ToF-SIMS spectra of $KHCO_3$, KNO_3, and KI standards that were obtained with an ion current such that the ^{39}K peak intensity was an order of magnitude higher than that given for the electrolytic cell sample. The saturation of the ^{39}K peak of the positive ToF-SIMS spectrum by the electrolytic cell sample is indicative of a unique crystalline matrix [11].

The negative ion ToF-SIMS of the electrolytic cell sample was dominated by H^-, and much smaller O^-, and OH^- peaks. A series of nonhydride containing negative ions $KCO_3[K_2CO_3]_n^-$ $m/z=(99+138n)$} was also present which implies that H_2 was eliminated from KH $KHCO_3$ during fragmentation of the compound KH $KHCO_3$.

3.2. XPS

A survey spectrum was obtained over the region $E_b=0$–1200 eV. The primary element peaks allowed for the determination of all of the elements present in each sample isolated from the K_2CO_3 electrolyte. The survey spectrum also detected shifts in the binding energies of potassium and oxygen which had implications as to the identity of the compound containing the elements. A high resolution XPS spectrum was also obtained of the low binding energy region ($E_b=0$–100 eV) to determine the presence of novel XPS peaks.

No elements were present in the survey scans which can be assigned to peaks in the low binding energy region with the exception of a small variable contaminant of sodium at 63 and 31 eV, potassium at 16.2 and 32.1 eV, and oxygen at 23 eV. Accordingly, any other peaks in this region must be due to novel species. The K 3s and K 3p are shown in Fig. 5 at 16.2 and 32.1 eV, respectively. A weak Na 2s is observed at 63 eV. The O 2s which is weak compared to the potassium peaks of K_2CO_3 is typically present at 23 eV, but is broad or obscured in Fig. 5. Peaks centered at 22.8 and 38.8 eV which do not correspond to any other primary element peaks were observed. The intensity and shift match shifted K 3s and K 3p. Hydrogen is the only element which does not have primary element peaks; thus, it is the only candidate to produce the shifted peaks. These peaks may be shifted by a highly binding hydride ion with a binding energy of

Table 2
The binding energies of XPS peaks of K_2CO_3 and an electrolytic cell sample

XPS	C 1s (eV)	O 1s (eV)	K 3p (eV)	K 3s (eV)	K $2p_{3/2}$ (eV)	K $2p_{1/2}$ (eV)	K 2s (eV)
K_2CO_3	288.4	532.0	18	34	292.4	295.2	376.7
Electrolytic	288.5	530.4	16.2	32.1	291.5	293.7	376.6
Cell		537.5	22.8	38.8	298.5	300.4	382.6
Sample		547.8					
Min	280.5	529			292		
Max	293	535			293.2		

22.8 eV given in the Appendix that bonds to potassium K 3p and shifts the peak to this energy. In this case, the K 3s is similarly shifted. These peaks were not present in the case of the XPS of matching samples isolated from an identical electrolytic cell except that Na_2CO_3 replaced K_2CO_3 as the electrolyte.

XPS further confirmed the ToF-SIMS data by showing shifts of the primary elements. The splitting of the principal peaks of the survey XPS spectrum is indicative of multiple forms of bonding involving the atom of each split peak. For example, the XPS survey spectrum shown in Fig. 6 shows extraordinary potassium and oxygen peak shifts. All of the potassium primary peaks are shifted to about the same extent as that of the K 3s and K 3p. In addition, extraordinary O 1s peaks of the electrolytic cell sample were observed at 537.5 and 547.8 eV; whereas, a single O 1s was observed in the XPS spectrum of K_2CO_3 at 532.0 eV. The results are not due to uniform charging as the internal standard C 1s remains the same at 284.6 eV. The results are not due to differential charging because the peak shapes of carbon and oxygen are normal, and no tailing of these peaks was observed. The binding

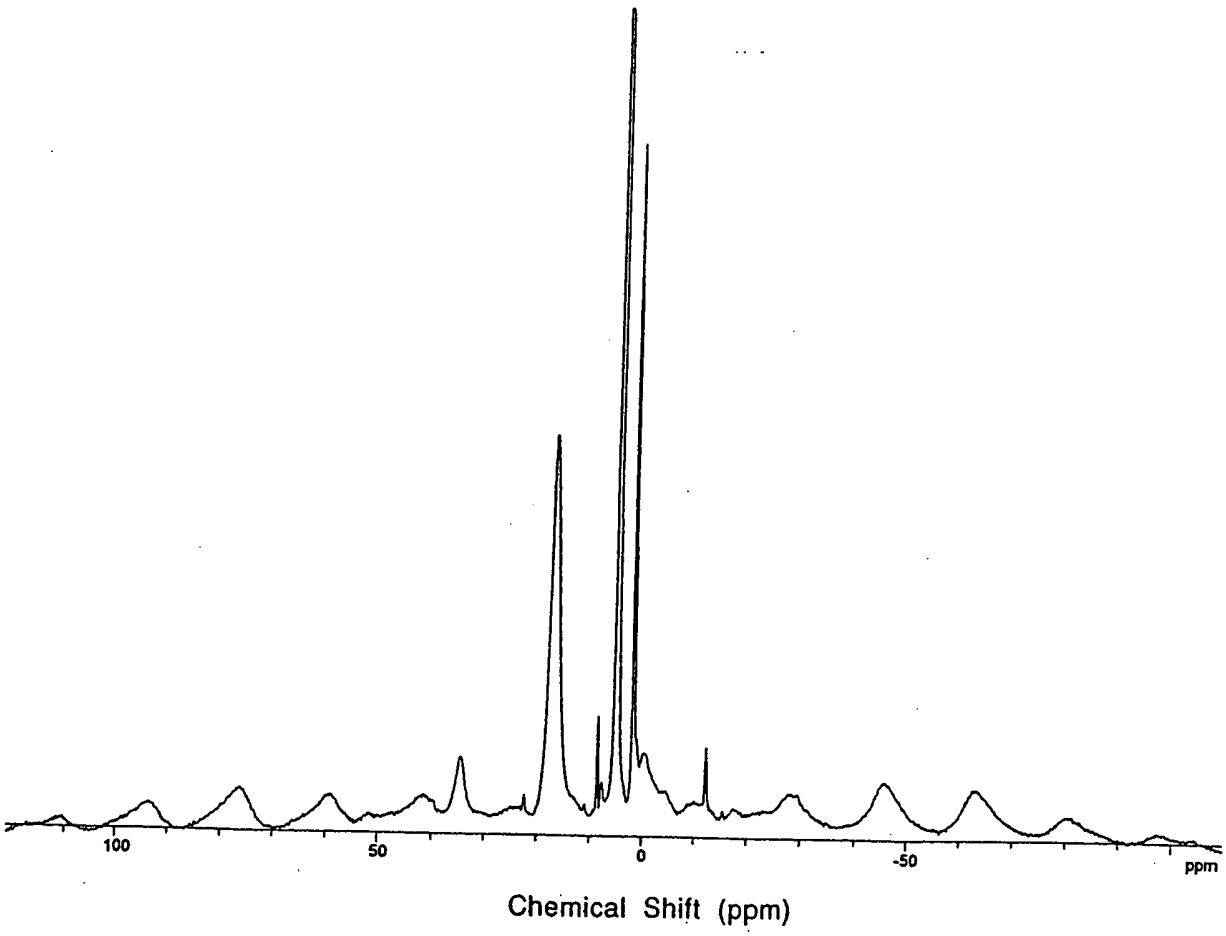

Fig. 7. The magic angle spinning proton NMR spectrum of an electrolytic cell sample.

Table 3
The NMR peaks of an electrolytic cell sample with their assignments

Peak at shift (ppm)	Assignment
+34.54	Side band of +17.163 peak
+22.27	Side band of +5.066 peak
+17.163	KH $KHCO_3$
+10.91	KH $KHCO_3$
+8.456	KH $KHCO_3$
+7.50	KH $KHCO_3$
+5.066	H_2O
+1.830	KH $KHCO_3$
−0.59	Side band of +17.163 peak
−12.05	KH $KHCO_3$ [a]
−15.45	KH $KHCO_3$

[a] A small shoulder is observed on the −12.05 peak which is the side band of the +5.066 peak.

energies of the K_2CO_3 control and an electrolytic cell sample are shown in Table 2. The range of binding energies from the literature [12] for the peaks of interest are given in the final row of Table 2. The K 3p, K 3s, K $2p_{3/2}$, K $2p_{1/2}$, and K 2s XPS peaks and the O 1s XPS peaks shifted to an extent greater than those of known compounds may correspond to and identify KH $KHCO_3$.

3.3. NMR

The signal intensities of the ^1H MAS NMR spectrum of the K_2CO_3 reference were relatively low. It contained a water peak at 1.208 ppm, a peak at 5.604 ppm, and very broad weak peaks at 13.2 and 16.3 ppm. The ^1H MAS NMR spectrum of the $KHCO_3$ reference contained a large peak at 4.745 with a small shoulder at 5.150 ppm, a broad peak at 13.203 ppm, and small peak at 1.2 ppm.

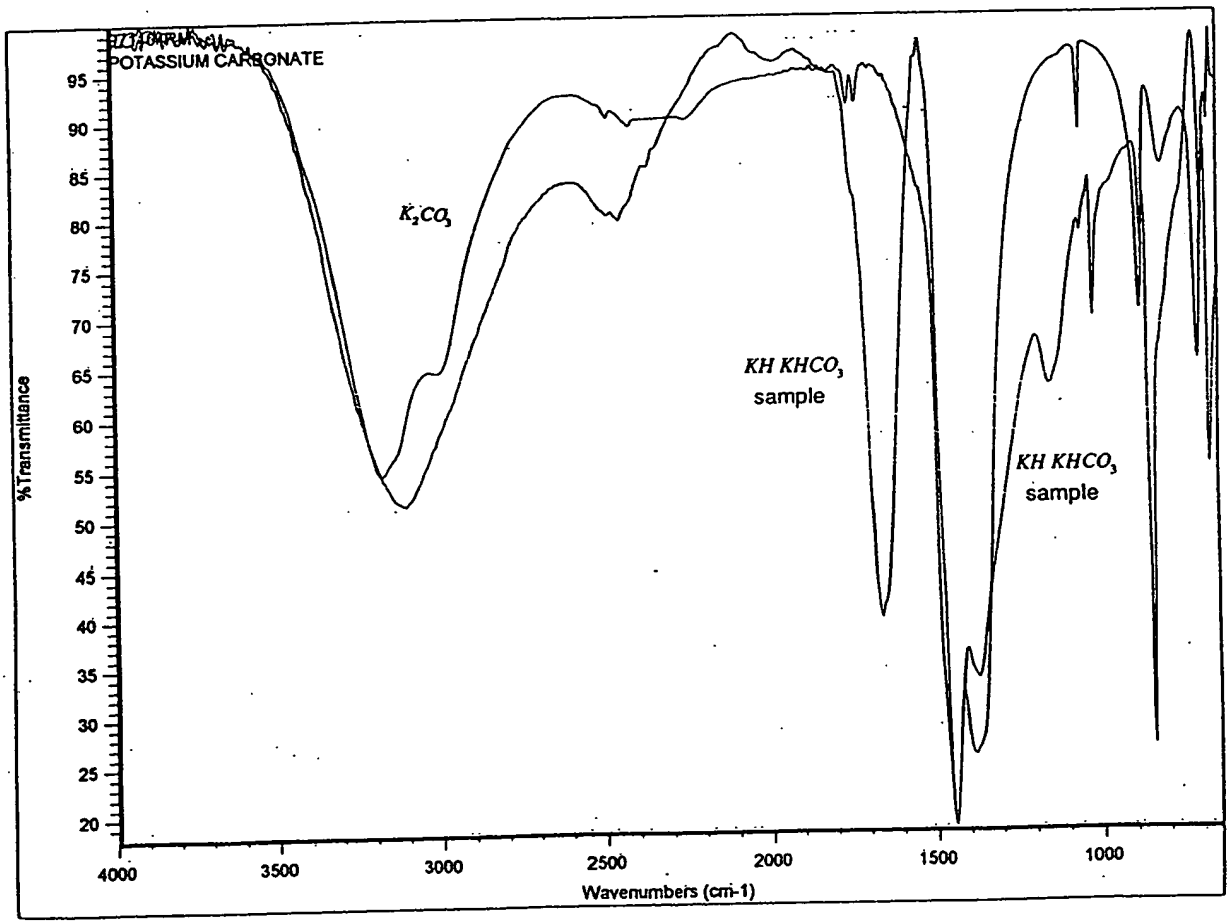

Fig. 8. The overlap FTIR spectrum of an electrolytic cell sample and the FTIR spectrum of the reference potassium carbonate.

The ^1H MAS NMR spectra of an electrolytic cell sample is shown in Fig. 7. The peak assignments are given in Table 3. The reproducible peaks assigned to KH $KHCO_3$ in Table 3 were not present in the controls except for the peak assigned to water at +5.066 ppm. The novel peaks could not be assigned to hydrocarbons. Hydrocarbons were not present in the electrolytic cell sample based on the ToF-SIMS spectrum and FTIR spectra which were also obtained (see below). The novel peaks without identifying assignment are consistent with KH $KHCO_3$. The NMR peak of the hydride ion of potassium hydride was observed at −0.376 ppm relative to TMS. The upfield peaks of Fig. 7 are assigned to novel hydride ion (KH-) in different environments. The down field peaks are assigned to the proton of the potassium hydrogen carbonate species in different chemical environments (-$KHCO_3$).

3.4. FTIR

The FTIR spectra of K_2CO_3 (99%) and $KHCO_3$ (99.99%) were compared with that of an electrolytic cell sample. A spectrum of a mixture of the bicarbonate and the carbonate was produced by digitally adding the two reference spectra. The two standards alone and the mixed standards were compared with that of the electrolytic cell sample. From the comparison, it was determined that the electrolytic cell sample contained potassium carbonate but did not contain potassium bicarbonate. The unknown component could be a bicarbonate other than potassium bicarbonate. The spectrum of potassium carbonate was digitally subtracted from the spectrum of the electrolytic cell sample. Several bands were observed including bands in the 1400–1600 cm^{-1} region. Some organic nitrogen compounds (e.g. acrylamides, pyrolidinones) have strong bands in the region 1660 cm^{-1} [13]. However, the lack of any detectable C=H bands (≈2800–3000 cm^{-1}) and the bands present in the 700–1100 cm^{-1} region indicate an inorganic material [14]. Peaks not assignable to potassium carbonate were observed at 3294, 3077, 2883, 1100, 2450, 1660, 1500, 1456, 1423, 1300, 1154, 1023, 846, 761, and 669 cm^{-1}.

The overlap FTIR spectrum of the electrolytic cell sample and the FTIR spectrum of the reference potassium carbonate appears in Fig. 8. In the 700–2500 cm^{-1} region, the peaks of the electrolytic cell sample closely resemble those of potassium carbonate, but they are shifted about 50 cm^{-1} to lower frequencies. The shifts are similar to those observed by replacing potassium (K_2CO_3) with rubidium (Rb_2CO_3) as demonstrated by comparing their IR spectra [15]. The shifted peaks may be explained by a polymeric structure for the compound KH $KHCO_3$ identified by ToF-SIMS, XPS, and NMR.

3.5. Further analytical tests

X-ray diffraction (XRD), elemental analysis using inductively coupled plasma (ICP), and Raman spectroscopy were also performed on the electrolytic sample [10]. The XRD data indicated that the diffraction pattern of the electrolytic cell sample does not match that of either KH, $KHCO_3$, K_2CO_3, or KOH. The elemental analysis supports KH $KHCO_3$. In addition to the known Raman peaks of $KHCO_3$ and a small peak assignable to K_2CO_3, unidentified peaks at 1685 and 835 cm^{-1} were present. Work in progress [10] demonstrates that KH $KHCO_3$ may also be formed by a reaction of gaseous KI with atomic hydrogen in the presence of K_2CO_3. In addition to the previous analytical studies, the fragment $KK_2CO_3^+$ corresponding to KH $KHCO_3$ was observed by electrospray ionization time of flight mass spectroscopy as a chromatographic peak on a C18 liquid chromatography column typically used to separate organic compounds. No chromatographic peaks were observed in the case of inorganic compound controls KI, $KHCO_3$, K_2CO_3, and KOH.

4. Discussion

Alkali and alkaline earth hydrides react violently with water to release hydrogen gas which subsequently ignites due to the exothermic reaction with water. Typically metal hydrides decompose upon heating at a temperature well below the melting point of the parent metal. These saline hydrides, so called because of their saltlike or ionic character, are the monohydrides of the alkali metals and the dihydrides of the alkaline-earth metals, with the exception of beryllium. BeH_2 appears to be a hydride with bridge type bonding rather than an ionic hydride. Highly polymerized molecules held together by hydrogen-bridge bonding is exhibited by boron hydrides and aluminum hydride. Based on the known structures of these hydrides, the ToF-SIMS hydride clusters such as $K[KH\,KHCO_3]_n^+$, the XPS peaks observed at 22.8 and 38.8 eV, upfield NMR peaks assigned to hydride ion, and the shifted FTIR peaks, the present novel hydride compound may be a polymer, $[KH\ KHCO_3]_n$, with a structural formula which is similar to boron and aluminum hydrides. The reported novel compound appeared polymeric in the concentrated electrolytic solution and in distilled water. $[KH\ KHCO_3]_n$ is extraordinarily stable in water; whereas, potassium hydride reacts violently with water.

As an example of the structures of this compound, the $K[KH\,KHCO_3]_n^+$ $m/z=(39+140n)$ series of fragment peaks is tentatively assigned to novel hydride bridged or linear potassium bicarbonate compounds having a general formula such as $[KH\,KHCO_3]_n$ n = 1,2,3 ... General structural formulas may be

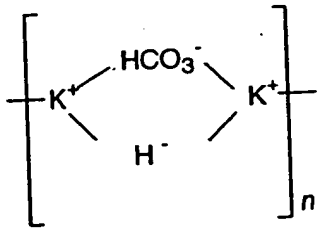

and

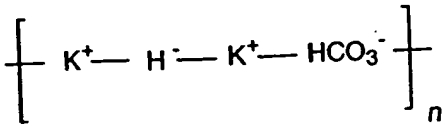

Liquid chromatography/ESIToFMS studies are in progress to support the polymer assignment.

The observation of inorganic hydride fragments such as $K[KH\,KHCO_3]^+$ in the positive ToF-SIMS spectra of samples isolated from the electrolyte following acidification indicates the stability of the novel potassium hydride potassium bicarbonate compound [10]. The electrolyte was acidified with HNO_3 to pH=2 and boiled to dryness to prepare samples to determine whether $KH\,KHCO_3$ was reactive under these conditions. Ordinarily no K_2CO_3 would be present, and the sample would be converted to KNO_3. Crystals were isolated by dissolving the dried crystals in water, concentrating the solution, and allowing crystals to precipitate. ToF-SIMS was performed on these crystals. The positive spectrum contained elements of the series of inorganic hydride clusters $\{K[KH\,KHCO_3]_n^+$ $m/z=(39+140n)$, $K_2OH[KH\,KHCO_3]_n^+$ $m/z=(95+140n)$, and $K_3O[KH\,KHCO_3]_n^+$, $m/z=(133+140n)\}$ that were observed in the positive ToF-SIMS spectrum of the electrolytic cell sample as discussed in the ToF-SIMS Results Section and given in Figs. 3 and 4 and Table 1. The presence of bicarbonate carbon (C 1s≅289.5 eV) was observed in the XPS of the sample from the HNO_3 acidified electrolyte. In addition, fragments of compounds formed by the displacement of hydrogen carbonate by nitrate were observed [10]. A general structural formula for the reaction maybe

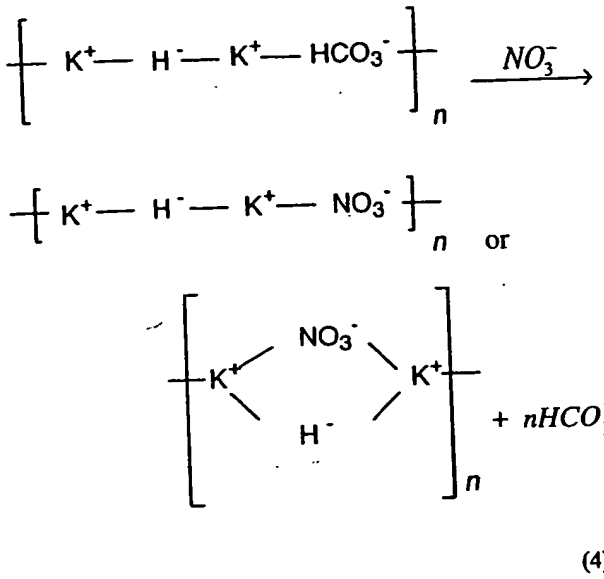

(4)

During acidification of the K_2CO_3 electrolyte the pH repetitively increased from 3 to 9 at which time additional acid was added with carbon dioxide release. The increase in pH (release of base by the titration reactant) was dependent on the temperature and concentration of the solution. A reaction consistent with this observation is the displacement reaction on NO_3^- for HCO_3^{2-} as given by Eq. (4).

5. Conclusions

The ToF-SIMS, XPS, and NMR results confirm the identification of $KH\,KHCO_3$ with a new state of hydride ion. The chemical structure and properties of this compound having a hydride ion with a high binding energy are indicative of a new field of hydride chemistry. The novel hydride ion may combine with other cations such as other alkali cations and alkaline earth, rare earth, and transition element cations. Thousands of novel compounds may be synthesized with extraordinary properties relative to the corresponding compounds having ordinary hydride ions. These novel compounds may have a breath of applications. For example a high voltage battery (Eqs. (1–3)) according to the hydride binding energy of 22.8 eV observed by XPS may be possible having projected specifications that surpass those of the internal combustion engine.

Acknowledgements

Special thanks to Bala Dhandapani of BlackLight Power, Inc., for work on the Raman, FTIR, and XRD studies. Special thanks to Jiliang He of BlackLight

Power, Inc., for obtaining the MAS NMR spectrum of potassium hydride. Special thanks to Robert Braun of BlackLight Power, Inc., Bala Dhandapani, and Jiliang He for helpful comments upon review of the manuscript.

Appendix A

A novel hydride ion having extraordinary chemical properties given by Mills [10] is predicted to form by the reaction of an electron with a hydrino (Eq. (A2)), a hydrogen atom having a binding energy given by

$$\text{Binding energy} = \frac{13.6\,\text{eV}}{\left(\frac{1}{p}\right)^2} \tag{A1}$$

where p is an integer greater than 1, designated as

$$\text{H}\left[\frac{a_H}{p}\right]$$

where a_H is the radius of the hydrogen atom. The resulting hydride ion is referred to as a hydrino hydride ion, designated as $H^-(1/p)$.

$$\text{H}\left[\frac{a_H}{p}\right] + e^- \rightarrow H^-(1/p) \tag{A2}$$

The hydrino hydride ion is distinguished from an ordinary hydride ion having a binding energy of 0.8 eV. The latter is hereafter referred to as "ordinary hydride ion". The hydrino hydride ion is predicted [10] to comprise a hydrogen nucleus and two indistinguishable electrons at a binding energy according to the following formula:

$$\text{Binding energy} = \frac{\hbar^2\sqrt{s(s+1)}}{8\mu_e a_0^2\left[\frac{1+\sqrt{s(s+1)}}{p}\right]^2} - \frac{\pi\mu_0 e^2\hbar^2}{m_e^2 a_0^3}\left(1+\frac{2^2}{\left[\frac{1+\sqrt{s(s+1)}}{p}\right]^3}\right) \tag{A3}$$

where p is an integer greater than one, $s = 1/2$, π is pi, $\hbar$ is Planck's constant bar, μ_0 is the permeability of vacuum, m_e is the mass of the electron, μ_e is the reduced electron mass, a_0 is the Bohr radius, and e is the elementary charge. The ionic radius is

$$r_1 = \frac{a_0}{p}(1+\sqrt{s(s+1)}); \quad s = \frac{1}{2} \tag{A4}$$

From Eq. (A4), the radius of the hydrino hydride ion $H^-(1/p)$; p = integer is $1/p$ that of ordinary hydride ion, $H^-(1/1)$. The XPS peaks centered at 22.8 and 38.8 eV are assigned to shifted K 3s and K 3p. The anion does not correspond to any other primary element peaks; thus, it may correspond to the $H^-(n=1/6)$ $E_b = 22.8$ eV hydride ion predicted by Mills [10] where E_b is the predicted binding energy.

Hydrinos are predicted to form by reacting an ordinary hydrogen atom with a catalyst having a net enthalpy of reaction of about

$$m\,27.21\,\text{eV} \tag{A5}$$

where m is an integer [10]. This catalysis releases energy from the hydrogen atom with a commensurate decrease in size of the hydrogen atom, $r_n = na_H$. For example, the catalysis of $H(n=1)$ to $H(n=1/2)$ releases 40.8 eV, and the hydrogen radius decreases from a_H to $1/2a_H$. One such catalytic system involves potassium. The second ionization energy of potassium is 31.63 eV; and K^+ releases 4.34 eV when it is reduced to K. The combination of reactions K^+ to K^{2+} and K^+ to K, then has a net enthalpy of reaction of 27.28 eV, which is equivalent to $m = 1$ in Eq. (A5).

$$27.28\,\text{eV} + K^+ + K^+ + \text{H}\left[\frac{a_H}{p}\right] \rightarrow K + K^{2+} + \text{H}\left[\frac{a_H}{(p+1)}\right] + [(p+1)^2 - p^2]\,13.6\,\text{eV} \tag{A6}$$

$$K + K^{2+} \rightarrow K^+ + K^+ + 27.28\,\text{eV} \tag{A7}$$

The overall reaction is

$$\text{H}\left[\frac{a_H}{p}\right] \rightarrow \text{H}\left[\frac{a_H}{(p+1)}\right] + [(p+1)^2 - p^2]\,13.6\,\text{eV} \tag{A8}$$

The energy given off during catalysis is much greater than the energy lost to the catalyst. The energy released is large as compared to conventional chemical reactions. For example, when hydrogen and oxygen gases undergo combustion to form water

$$H_2(g) + \frac{1}{2}O_2(g) \rightarrow H_2O(l) \tag{A9}$$

the known formation enthalpy of water is $\Delta H_f = -286$ kJ/mole or 1.48 eV per hydrogen atom. By contrast, each ordinary hydrogen atom ($n = 1$) catalysis releases a net of 40.8 eV. The exothermic reactions Eqs. (A6)–(A8), Eq. (A2) and the enthalpy of formation of KH $KHCO_3$ could explain the observation of excess enthalpy of 1.6×10^9 J that exceeded the total input enthalpy given by the product of the electrolysis voltage and current over time by a factor greater than 8 [7].

References

[1] Uehara I, Sakai T, Ishikawa H. J Alloy Comp 1997;253/254:635–41.

[2] Glanz J. Check the tires and charge her up, New Scientist, April 15, pp. 32–35, 1995.

[3] Mulholland D. Defense News, Powering the Future Military, March 8, pp. 1 & 34, 1999.

[4] Aceves SM, Berry GD, Rambach GD. Int J Hydrogen Energy 1998;23(7):583–91.

[5] Ball J. Auto makers are racing to market "green" cars powered by fuel cells, The Wall Street Journal, March 15, p. 1, 1999.

[6] National Technical Information Service, US Department of Commerce. Advanced automotive technology: visions of a super-efficient family car, US Office of Technology Assessment, Washington, DC PB96-109202, September 1995.

[7] Mills R, Good W, Shaubach R. Fusion Technol 1994;25:103.

[8] Microsc Microanal Microstruct, Vol. 3, 1, 1992.

[9] PHI Trift II, ToF-SIMS Technical Brochure, Eden Prairie, MN 55344, 1999.

[10] Mills R. The grand unified theory of classical quantum mechanics, January ed. Cranbury, New Jersey: BlackLight Power, Inc, 1999 Distributed by Amazon.com.

[11] Practical surface analysis. In: Briggs D, Seah MP, editors. Ion and neutral spectroscopy, 2nd ed. Wiley and Sons, New York, 1992. 2.

[12] Wagner CD, Riggs WM, Davis LE, Moulder JF, Mulilenberg GE, editors. Handbook of X-ray photoelectron spectroscopy. Eden Prairie, Minnesota: Perkin–Elmer Corp, 1997.

[13] Lin-Vien D, Colthup NB, Fateley WG, Grassellic JG. The handbook of infrared and Raman characteristic frequencies of organic molecules. Academic Press, Inc, 1991.

[14] Nyquist RA, Kagel RO, editors. Infrared spectra of inorganic compounds. New York: Academic Press, 1971.

[15] Brooker MH, Bates JB. Spectrochimica Acta 1994;30A:2211–20.